Defense-related callose synthase *PMR4* promotes root hair callose deposition and adaptation to phosphate deficiency in *Arabidopsis thaliana*

1 Kentaro Okada[1,2], Koei Yachi[1], Tan Anh Nhi Nguyen[1], Satomi Kanno[3], Chika Tateda[1],
2 Tae-Hong Lee[1], Uyen Nguyen[4], Shunsuke Miyashima[1], Kei Hiruma[1], Kyoko Miwa[5],
3 Takaki Maekawa[4, 6], Michitaka Notaguchi[2], Yusuke Saijo[1]

4 [1]Graduate School of Science and Technology, Nara Institute of Science and
5 Technology, Takayama-cho, Ikoma 630-0192, Japan
6 [2]Bioscience and Biotechnology Center, Nagoya University, Furo-cho, Chikusa-ku,
7 Nagoya 464-8601, Japan.
8 [3]Institute for Advanced Research, Nagoya University, Furo-cho, Chikusa, Nagoya 464-
9 8601, Japan
10 [4]Institute for Plant Sciences, University of Cologne, Cologne D-50674, Germany
11 [5]Graduate School of Environmental Science, Hokkaido University, Sapporo 060-0810,
12 Japan
13 [6]CEPLAS Cluster of Excellence on Plant Sciences at the University of Cologne,
14 Cologne D-50674, Germany
15

Author for correspondence: Yusuke Saijo
ORCID ID: 0000-0001-8985-9695
Tel: +81-743-72-5690
Email: saijo@bs.naist.jp

Summary

Plants acquire phosphorus (P) primarily as inorganic phosphate (Pi) from the soil. Under Pi deficiency, plants induce an array of physiological and morphological responses, termed phosphate starvation responses (PSR), thereby increasing Pi acquisition and use efficiency. However, the mechanisms underlying and finetuning PSR remain to be elucidated. Here, we report that deposition of a β-1,3-glucan polymer called callose is induced in *Arabidopsis thaliana* root hairs under Pi deficiency, in a manner independent of *PHR1/PHL1* transcription factors and *LPR1/LPR2* ferroxidases, mediating systemic and local PSR, respectively. A mutagenic screen has revealed *PMR4* (*GSL5*) callose synthase being required for the callose deposition under Pi deficiency. Loss of *PMR4* also affects different PSR-characteristic outputs, including phosphate mobilization, plant growth and anthocyanin accumulation, indicating a critical role for *PMR4*-dependent callose in PSR. The PSR defects are not affected by simultaneous disruption of *SID2*, mediating defense-associated salicylic acid (SA) biosynthesis, unlike SA-dependent powdery mildew resistance previously described in *pmr4*. Grafting analyses and genetic studies on root hair-defective mutants suggest that *PMR4*-dependent callose deposition in the root hairs contributes to shoot Pi accumulation during PSR. Our findings thus illuminate an important role for *PMR4* in plant adaptation to Pi deficiency.

Key words: cell wall, nutrient deficiency, pattern triggered immunity, phosphate transport, powdery mildew resistance, salicylic acid (SA)

38 **Introduction**

39 As an essential macronutrient, plants acquire and distribute P from the rhizosphere to
40 the whole tissues, primarily in the form of inorganic phosphate (Pi). To maintain Pi
41 homeostasis under Pi deficiency, plants induce a series of adaptive responses, *e.g.*
42 increasing Pi uptake, remobilization and utilization, termed phosphate starvation
43 responses (PSRs), and also involve beneficial microbes in mutualistic associations
44 (Péret *et al*., 2011; Chien *et al*., 2018; Isidra-Arellano *et al*., 2021). PSR is accompanied
45 by extensive transcriptional reprogramming, mainly through the transcription factor
46 *PHR1* and related *PHL1*, which leads to increases in Pi transporter expression, root hair
47 formation and anthocyanin accumulation (Rubio *et al*., 2001, Bustos *et al*., 2010).
48 *PHR1/PHL1* mediate systemic coordination of these PSR-related events according to
49 the internal Pi availability. In addition, PSR also leads to remodeling root system
50 architecture, a decrease in primary root growth while increasing lateral root formation
51 and growth, through the ferroxidases *LPR1* and *LPR2* (Svistoonoff *et al*., 2007; Péret *et*
52 *al*., 2014; Balzergue *et al*., 2017). *LPR1/LPR2* are required for arresting primary root
53 growth when the external Pi levels are reduced surrounding the root tip (Svistoonoff *et*
54 *al*., 2007). Recent studies have pointed to an intimate relationship between PSR and
55 biotic interactions, but the molecular basis for their coordination remains poorly
56 understood (Chan *et al*., 2021).

57 Callose deposition on the plasma membrane through callose synthases *Glucan*
58 *Synthase Likes* (*GSLs*) reinforces barrier functions of the cell wall and restricts
59 plasmodesmatal permeability, in plant development and biotic/abiotic stress responses
60 (Jacobs *et al*., 2003; Nishimura *et al*., 2003; Dong *et al*., 2005; Enns *et al*., 2005;
61 Nishikawa *et al*., 2005; Chowdhury *et al*., 2014; Ellinger & Voigt, 2014; Sager & Lee,

62 2014; Wu *et al*., 2018). In *Arabidopsis thaliana,* callose deposition is induced in the
63 root phloem in response to excess iron, thereby reducing plasmodesmatal permeability
64 (O'Lexy *et al*., 2018). Of 12 *Arabidopsis thaliana GSLs*, *GSL2* (*CALS5*) and *GSL5*
65 (*PMR4, CALS12*) respectively contribute to basal accumulation and iron-induced
66 deposition of callose in the root phloem (O'Lexy *et al*., 2018). Callose also accumulates
67 in the stem cell niche (SCN) surrounding the quiescent center cells, thereby inhibiting
68 cell-to-cell movement of the transcription factor SHORT ROOT (SHR) during PSR.
69 This serves to suppress cell division and elongation in the root apical meristem and
70 elongation zone, respectively, through the *LPR1/LPR2* pathway (Müller *et al*., 2015;
71 Mora-Macías *et al*., 2017). *GSL5* (*PMR4*) also mediates callose deposition in response
72 to pathogen challenge and microbe/damage-associated molecular patterns
73 (MAMPs/DAMPs), and promotes fungal penetration resistance (Wang *et al*., 2021).
74 However, the loss of *GSL5* function results in strong resistance to powdery mildew
75 fungi through tightened SA-based defenses, demonstrated by *gsl5* mutants revealed as
76 *powdery mildew resistance4* (*pmr4*) (Vogel & Somerville, 2000; Nishimura *et al*.,
77 2003). This resistance is thought to represent a backup defense activated when *GSL5*
78 (*PMR4*)-mediated callose deposition, a key output of MAMP/DAMP-triggered defense
79 signaling, is disrupted. Despite increasing knowledge, our understanding is still limited
80 for the possible involvement and significance of callose deposition in biotic and abiotic
81 stress responses.
82 Here, we report that callose deposition is induced in root hairs under Pi deficiency, in
83 a manner independent of *PHR1/PHL1* and *LPR1/LPR2*. Our mutagenic screen revealed
84 novel *pmr4* (*gsl5*) alleles among the mutants of the root-hair callose alteration under Pi
85 deficiency. The loss of *PMR4*-mediated callose deposition is associated with reduced

86 plant growth as well as exaggerated stress symptoms under Pi deficiency, in addition
87 with enhanced powdery mildew resistance. The results indicate *PMR4*-mediated callose
88 deposition in root hairs as a critical step in the acquisition and utilization of Pi during
89 PSR.
90
91 **Materials and Methods**
92 **Plant Materials and growth conditions**
93 *Arabidopsis thaliana* mutant materials were used in the accession Col-0 or Ws-2
94 background (Table S1). We generated ethyl methanesulfonate (EMS)-mutagenesis (M2)
95 seeds for screening. All seeds were sterilized using 6% sodium hypochlorite and 0.2%
96 Trion X-100 for 15 min, and then kept at 4°C for 2 d before sowing half-strength
97 Murashige and Skoog (MS) medium with 25 mM sucrose and 0.8% Agar (WAKO,
98 Japan). If not stated otherwise, the normal Pi medium contained 625 μM KH_2PO_4,
99 whereas the low Pi medium contained 50 μM KH_2PO_4. Plants were grown in a growth
100 chamber under 12 h: 12 h, light : dark cycles at 22°C. Six-d-old seedlings were
101 transferred to the indicated Pi liquid media or agar media with 1% Difco Agar,
102 Bacteriological (BD, Franklin Lakes, NJ, USA). For growth under different B
103 conditions, plants were grown in MGRL solid media containing 1% sucrose and 1%
104 gellan gum (WAKO, Japan). B concentrations were adjusted with boric acid. Plants
105 were grown under 16 h : 8 h, light : dark cycles at 22°C.
106
107 **Aniline blue staining**
108 Callose staining with aniline blue was conducted as described in Schenk & Schikora
109 (2015). Three d after the transfer of 5-d-old seedlings to the indicated Pi liquid media,

110 they were fixed in a solution containing acetic acid and ethanol (1:3 v/v) overnight. The
111 fixation solution was exchanged to a 150 mM K_2HPO_4 solution before callose staining
112 with 0.1% aniline blue in the K_2HPO_4 solution for 2 h. Callose signals were detected
113 under microscopy using a fluorescence microscope DMI 6000B (Leica) and a confocal
114 microscope SP8 (Leica).
115
116 **Inoculation analyses with powdery mildew fungi**
117 Inoculation of *Golovinomyces orontii* and determination of fungal versus plant DNA
118 ratio were conducted essentially by following Weßling & Panstruga (2012). Eighteen-d-
119 old plants grown in a 10 h : 14 h, light : dark cycle at 22°C were inoculated with *G.*
120 *orontii* spores at approximately 750 spores cm^{-2}. The inoculated leaves were harvested
121 and frozen in liquid nitrogen before determining fungal biomass at 10 d after
122 inoculation. Genomic DNA was extracted essentially by following Brouwer *et al*.
123 (2003). Quantitative real-time PCR was performed with primers (Table S2) and
124 Brilliant Sybr Green QPCR Reagent Kit (Stratagene, Waldbronn, Germany). The ratio
125 of *G. orontii* to Arabidopsis genomic DNA was calculated using the ΔΔCt method
126 (Pfaffl, 2001).
127
128 **Measurement of root hair density, primary root length and root area**
129 Six-d-old seedlings were transferred and further grown in the normal or low Pi media
130 for 6 d, and then the primary root apical area was observed under stereomicroscope
131 M80 (Leica). The number of root hairs was determined in a region 2.0-3.0 mm from the
132 root tip using Image J software (National Institutes of Health, Bethesda, MD, USA).

133 The primary root length and convex hull area were determined using ImageJ software
134 and Root nav software (Pound *et al*., 2013).
135
136 **Measurement of anthocyanin and Pi contents**
137 Six-d-old seedlings were transferred to the media of different Pi concentrations (10,
138 150, and 625 μM KH_2PO_4) and then further grown for 9 d. Shoot and root tissue was
139 ground in liquid Nitrogen to determine the anthocyanin and Pi contents. Anthocyanin
140 content was determined by following Mita (1997). In brief, after 1:99 (v/v), HCl :
141 methanol was added with 1 mL per sample, the homogenates were incubated at 4°C
142 overnight. A_{530} and A_{657} of the supernatant were measured by a spectrometer UV-1800
143 (Shimadzu, Kyoto, Japan). Anthocyanin content was calculated following the formula:
144 $(A_{530} - 0.25 \times A_{657}) \times$ fresh weight $(FW)^{-1}$.
145 Pi content was determined by following Ames (1966). In brief, the extraction buffer (10
146 mM Tris, 1 mM EDTA, 100 mM NaCl, 1mM phenylmethylsulfonyl fluoride pH8.0)
147 was added with 10 μL per sample mg FW. The homogenate 100 μl was mixed with 1%
148 glacial acetic acid 900 μl, and then incubated at 42°C for 30 min. The supernatant was
149 recovered to be incubated in a solution (0.35% NH_4MoO_4, 0.86 N H_2SO_4, and 1.4%
150 ascorbic acid) at 42°C for 30 min. A_{820} of the aliquot was measured under Eppendorf
151 BioSpectrometer® basic (Eppendorf). Then, Pi content was calculated by a P
152 calibration curve prepared with a P standard solution.
153
154 **Measurement of ^{32}P uptake rate and translocation ratio**
155 Seven-d-old seedlings were transferred to and further grown on the aforementioned Pi
156 media (50 or 625 μM KH_2PO_4) for 10 d. The seedlings were exposed to the liquid

157 media containing ^{32}P-labeled Pi ($^{32}PO_4^{3-}$ 20 kBq / ml) for 30 min. The plant tissues were
158 fixed to an Imaging Plate (GE Healthcare co.) for 3 h and then scanned by Typhoon
159 FLA 9000 (GE Healthcare co.). ^{32}P uptake rate was calculated based on a calibration
160 curve for ^{32}P. For determining the Pi translocation rate into shoots, the seedlings were
161 exposed to the Pi-containing liquid media containing ^{32}P-labeled Pi for 10 min, and then
162 transferred to non-labelled agar media for 120 min. The translocation rate of Pi was
163 determined by calculating ^{32}P ratio of the shoot to the whole seedlings.
164

165 **Grafting experiments**

166 Grafting of WT and *pmr4* was performed with a supportive micro-device as described
167 in Tsutsui *et al*. (2020). Four-d-old seedlings grown in a 1/2 MS medium containing
168 0.5% sucrose and 1% agar at 22°C were subject to grafting. Both hypocotyls of stock
169 and scion were cut horizontally with a knife and assembled on the device using forceps.
170 The grafted plants were grown in a 1/2 MS medium containing 0.5% sucrose and 2%
171 agar at 27°C for 6 d, and then transferred to the indicated Pi media (50 and 150 μM
172 KH_2PO_4) at 22°C for 9 d or 14 d for callose staining and shoot fresh weight (FW)
173 determination, respectively.
174

175 **Results**

176 **Callose deposition occurs in root hairs under phosphate deficiency, independently**
177 **of *PHR1/PHL1* and *LPR1/LPR2***

178 Under Pi deficiency, callose deposition was previously described in the root SCN
179 and cortex cells of the elongation zone (WT, Müller *et al*., 2015). In addition, we
180 noticed callose deposition in the epidermal cells, particularly in root hairs of the

181 differentiation zone (Fig. 1a, b; O'Lexy *et al*., 2018). However, callose deposition was
182 not detected in root hairs under the tested N, Fe or Fe/Pi deficient conditions (Fig. 1a).
183 The results indicate that the callose deposition is specific to Pi deficiency and is
184 dependent on Fe. The absence of callose staining in the epidermis of root hair-less *rhd6*
185 mutants (Fig. 1c) validated that callose deposition occurs in root hairs under low Pi. We
186 next assessed whether *PHR1/PHL1* and *LPR1/LPR2* play a role in the root hair callose
187 deposition. Although *LPR1* and *LPR2* contribute to the callose deposition in SCN
188 (Müller *et al*., 2015), the root hair callose deposition was not affected in *lpr1 lpr2* (Fig.
189 1c). Furthermore, wild type (WT)-like callose deposition was retained in root hairs of
190 *phr1 phl1 lpr1 lpr2* under low Pi conditions (Fig. 1c). The results indicate that callose
191 deposition is induced in root hairs under Pi deficiency independently of these PSR
192 pathways.
193
194 **Isolation of *callose alteration under Pi starvation* mutants**
195 To unravel genetic requirements for the callose deposition in root hairs under Pi
196 deficiency, we screened a total of 18,550 ethyl methane sulfonate (EMS)-mutagenized
197 individuals in Col-0 and Ler backgrounds. This revealed two mutants in the Col-0
198 background, designated *callose alteration under Pi starvation 1 and 2* (*caps1 and*
199 *caps2*, Fig. 2a). *caps1* and *caps2* mutants were severely defective in callose deposition
200 of root hairs under low Pi conditions (Fig. 2a). We also examined different *gsl* mutants
201 for possible alterations in callose deposition under these conditions. Of the tested *gsl*
202 mutants, *gsl5* (hereafter, *pmr4*) mutants specifically lacked callose deposition in root
203 hairs, like *caps1* and *caps2* mutants (Fig. 2a, Fig. S1). We therefore determined whether
204 the *caps* mutants carry a mutation(s) in *PMR4*, by sequencing the *PMR4* genomic

205 region. In both *caps1* and *caps*2, a DNA substitution was found within the *PMR4*
206 coding region (Fig. 2b). The mutation in *caps*1 converts Tryptophan to Stop codon at
207 the 260th amino acid (PMR4^{W260*}), resulting in PMR4 truncation that severely impairs
208 callose deposition as well as *pmr4-1* (PMR4^{W687*}). In *caps2*, Glutamic acid is
209 substituted with Lysine at the 1181st amino acid (PMR4^{E1181K}), which is within the
210 cytosolic side of a predicted glucan-synthase domain (residue 575 to 1558, orange-
211 marked domain, Fig. 2b). The results suggest that *PMR4* plays a key role in the
212 induction of root hair callose deposition under Pi deficiency. We validated that leaf
213 callose deposition in response to the bacterial MAMP flg22, a PTI output dependent on
214 *PMR4*, is abolished in these *caps* alleles (Fig S2). Moreover, we showed strong
215 resistance to powdery mildew fungi in these *caps* alleles (Fig. 2c, d), as previously
216 described in *pmr4* mutants (Vogel & Somerville, 2000; Nishimura *et al*., 2003). The
217 results indicate that *PMR4* is dysfunctional in both *caps* alleles.
218
219 ***PMR4* influences root development traits associated with PSR**
220 By using *pmr4-1* as a representative mutant allele, we further investigated the
221 functional significance of *PMR4* under Pi deficiency. The loss of *PMR4* leads to an
222 increase in salicylic acid (SA) biosynthesis and defense under biotic stress (Vogel &
223 Somerville, 2000; Nishimura *et al*., 2003), in a manner requiring *SID2 isochorismate*
224 *synthase* that mediates a critical step in SA biosynthesis during defense activation
225 (Wildermuth *et al*., 2001). Given the negative impact of SA on plant growth (Mateo *et*
226 *al*., 2006; Zhang *et al*., 2010), we assessed the possible SA dependence of the observed
227 *pmr4* phenotypes, by examining genetic interactions between *pmr4* and *sid2*. Callose
228 deposition was induced in *sid2* root hairs but not induced in *pmr4 sid2* under low Pi

229 conditions (Fig. 3a), demonstrating that *SID2*-mediated SA biosynthesis is not required
230 for *PMR4*-mediated callose deposition in root hairs.
231 In *Arabidopsis thaliana*, root hair cells specifically occur at the junction of two
232 underlying cortical cells, whereas non-hair cells occur in the other epidermal cells
233 (Dolan *et al.*, 1994; Schiefelbein *et al.*, 2009). Root hair density was increased under
234 low Pi conditions compared to normal Pi conditions, and the increase was exaggerated
235 in *pmr4* as well as *pmr4 sid2*, without ectopic root hair formation (Fig. 3b-d). Likewise,
236 root hair length was also increased in *pmr4* as well as *pmr4 sid2* under both Pi
237 conditions (Fig. 3c, d). The results suggest that *PMR4* is not required for the
238 differentiation or outgrowth of root hair cells, but that *PMR4* contributes to restricting
239 root hair formation and elongation, in the presence or absence of *SID2*. Conversely,
240 primary root length was reduced in *pmr4* compared with WT in both low and normal Pi
241 conditions (Fig. 3b, e). We then determined the ratio of the primary root length under
242 normal Pi versus low Pi as an indicator for the primary root growth inhibition under Pi
243 deficiency. The ratio (normal/low Pi) was increased in *pmr4* compared with WT,
244 indicating that primary root growth inhibition, a proxy in PSR, is exaggerated in *pmr4*
245 (Fig. 3f). Importantly, the primary root growth inhibition was not affected in *sid2*, but
246 again exaggerated in *pmr4 sid2* (Fig. 3e, f), indicating that the enhancement in the Pi
247 starvation-induced response of *pmr4* is independent of *SID2*-mediated SA biosynthesis.
248 We further examined whether *PMR4* influences the primary root growth inhibition
249 under boron (B) scarcity (Miwa *et al.*, 2013). Although the primary root length was
250 reduced in *pmr4* compared to WT over the tested range of B concentrations, its ratio
251 under B sufficiency (100 μM) versus the examined low B conditions was not affected in
252 *pmr4* (Fig. S3), pointing to specific contribution of *PMR4* to PSR.

253 Since the primary root growth inhibition during PSR relies on *LPR1* and *LPR2*
254 (Svistoonoff *et al*., 2007; Müller *et al*., 2015), we examined the possible relationship
255 between *LPR1/LPR2* and *PMR4* in the regulation of the primary root growth. The
256 primary root length was reduced in *pmr4 lpr1 lpr2* compared with *lpr1 lpr2* under both
257 Pi conditions, whereas it was increased in *pmr4 lpr1 lpr2* compared with *pmr4*
258 specifically under low Pi (Fig. S4). The results indicate that *PMR4* serves to sustain the
259 primary root growth irrespective of the Pi availability or *LPR1/LPR2* inhibition activity,
260 whereas the *LPR1/LPR2* function is significant specifically under low Pi in the presence
261 or absence of *PMR4*. The ratio of the primary root length under normal Pi versus low Pi
262 was lowered to a similar extent in *lpr1 lpr2* and *pmr4 lpr1 lpr2* compared with WT,
263 despite the decrease in the primary root length by *pmr4* (Fig. S4), indicating that *lpr1*
264 *lpr2* is epistatic to *pmr4*.
265 We next determined the convex hull root area as a proxy of overall root system
266 growth, which was correlated with Pi availability (Fig. 3g). It was reduced in *pmr4* and
267 *sid2* compared with WT under both normal and low Pi conditions, albeit to a lesser
268 extent in *sid2* than *pmr4* under low Pi (Fig. 3g), suggesting that *PMR4* and *SID2* both
269 serve to expand the root area. Notably, only in the presence of *SID2*, the root area under
270 both Pi conditions and its normal/low Pi ratio were respectively reduced and increased
271 in *pmr4* relative to WT (Fig. 3g, h), suggesting that *SID2* positively influences *PMR4*
272 promotion of the root system expansion. Conversely, the root area was greater in *pmr4*
273 *sid2* compared to *pmr4* under low Pi (Fig. 3g), suggesting that a negative impact of
274 *SID2* on root expansion becomes apparent specifically when *PMR4* is disrupted during
275 PSR.
276

277 ***PMR4* serves to sustain shoot growth and restrict anthocyanin accumulation under**
278 **Pi deficiency.**
279 We next examined whether *PMR4* influences shoot growth, by determining shoot
280 fresh weight (FW), under Pi deficiency. Shoot FW was lowered in *pmr4* compared with
281 WT, and it was not even partially restored by the simultaneous loss of *SID2* in *pmr4*
282 *sid2* under low-Pi media or soil (Fig. 3i-j, Fig. S5). Together with the root phenotypes
283 described above, the results exclude *SID2* as the major cause of the growth inhibition in
284 *pmr4*. The results suggest that *PMR4* positively influences shoot growth in the presence
285 of *SID2*, and that *SID2* did not reduce shoot growth under low Pi. Although high SA
286 accumulation was described to reduce plant growth (Miura *et al*., 2010), we did not
287 detect negative impacts of *SID2* on shoot growth under both Pi conditions.
288 Anthocyanin content was increased in *pmr4* compared with WT, in the presence or
289 absence of *SID2* (Fig. 3k, l). Although SA was described to enhance anthocyanin
290 accumulation under Pi starvation (Morcillo *et al*., 2019), *sid2* was largely
291 indistinguishable from WT in anthocyanin contents under our low Pi conditions (Fig.
292 3k, l). The results suggest that *PMR4* suppresses excessive anthocyanin accumulation
293 under Pi deficiency in a manner independent of *SID2*.
294
295 ***PMR4* promotes the acquisition and root-to-shoot translocation of Pi**
296 The *PMR4* effects on shoot and root growth prompted us to examine its possible role
297 in Pi acquisition from the rhizosphere and Pi mobilization within the plant. We found
298 that shoot Pi concentrations were greatly reduced in *pmr4* compared with WT, without
299 alterations in root Pi concentrations, under Pi deficiency (Fig. 4a, b). This indicates that
300 *PMR4* contributes to Pi accumulation in shoots during PSR. It was described that

301 *PHR1/PHL1* promotes shoot Pi accumulation (Wang *et al*., 2018) and that *PHO1* Pi
302 transporter mediates Pi mobilization from roots to shoots through the root xylem vessels
303 (Stefanovic *et al*., 2007). We validated that Pi contents were lowered in the shoots but
304 increased in the roots, in *phr1 phl1* and *pho1* compared with WT under low Pi (Fig. 4c).
305 A decrease in shoot Pi contents was also observed in *phr1 phl1* and *pho1* under normal
306 Pi (Fig. 4d). Since root hairs contribute to Pi accumulation under Pi deficiency (Tanaka
307 *et al*., 2014; Robertson-Albertyn *et al*., 2017; Holz *et al*., 2018), we next determined Pi
308 contents in a root hair less mutant, *rhd6* (Fig. 4c, d). As seen in *pmr4, phr1 phl1* and
309 *pho1*, Pi contents were lowered in the shoots but not in the roots of *rhd6* compared to
310 WT specifically under Pi deficiency (Fig. 4c-d). In sum, all these mutants displayed a
311 decrease in shoot Pi contents without affecting or reducing root Pi contents under Pi
312 deficiency (Fig 4e). We inferred from these results that *PMR4*-mediated callose
313 deposition in root hairs contributes to shoot Pi accumulation, possibly through
314 increasing the uptake or root-to-shoot translocation of Pi. To test the hypothesis, we
315 determined the rates of Pi uptake and Pi translocation by applying and tracing radio-
316 labelled P. The ratio of ^{32}P contents in the shoot to whole seedling stands for Pi
317 translocation rate. The rate of ^{32}P uptake per time and the ratio of ^{32}P in the shoot to
318 whole seedling were both lowered in *pmr4* and *pmr4 sid2* compared to WT and *sid2,*
319 respectively, under low Pi (Fig. 4f, g). In the presence of *SID2*, *PMR4* contribution to
320 the two proxies was significant only under low Pi (Fig. 4f, g). In the absence of *SID2*
321 however, *PMR4* contribution to P uptake was apparent under normal Pi as well (Fig.
322 4f). Moreover, the ^{32}P uptake rate was reduced in *sid2* compared to WT, whereas *pmr4*
323 *sid2* was not distinguishable from *pmr4* under low Pi (Fig. 4f), suggesting that *SID2*
324 positively influences Pi uptake during PSR in the presence of *PMR4*. These results

325 suggest that *PMR4* promotes Pi uptake and root-to-shoot Pi translocation under Pi
326 deficiency, and that the former but not the latter *PMR4* function is dependent on *SID2*.
327
328 **Root *PMR4* contributes to shoot growth under Pi deficiency**
329 We next examined the significance of root *PMR4* in promoting shoot growth,
330 through micrografting between WT and *pmr4* mutants. We validated that the
331 micrografted plants of WT/WT (shoot/root genotypes) and *pmr4/pmr4* showed the
332 corresponding WT and *pmr4* phenotypes in root growth and SFW (Fig. 5a, b) and that
333 the root hair callose was detected only when *PMR4* was present in the roots (Fig. 5d).
334 Remarkably, SFW was greatly reduced in WT/*pmr4* whereas it was less affected in
335 *pmr4*/WT (Fig. 5b), pointing to a critical role for a root *PMR4* pool in shoot growth
336 during PSR. However, the root growth was partially restored in WT/*pmr4* (Fig. 5c),
337 pointing to a role for a shoot *PMR4* pool in sustaining the primary root growth during
338 PSR.
339
340 **Discussion**
341 Our studies on callose deposition in root hairs induced under Pi deficiency led to the
342 discovery of *PMR4* as a key regulator of PSR (Fig. 6). *PMR4* mediates defense-induced
343 callose deposition in pattern triggered immunity and pre-invasion fungal resistance
344 (Jacobs *et al*., 2003; Chowdhury *et al*., 2014), and that its loss is linked to enhanced SA-
345 based pathogen resistance (Nishimura *et al*., 2003). By revealing different *caps* (*gsl5,*
346 *pmr4*) alleles, we show that the disruption of *PMR4* results in the loss of root-hair
347 callose deposition, in addition to powdery mildew resistance and a lack for callose

348 deposition during PTI. Therefore, *PMR4* seems to play a critical role in an array of
349 biotic and abiotic stress responses, possibly through callose deposition at different sites.
350 Our results suggest that the root hair callose contributes to PSR, by promoting root Pi
351 uptake and shoot Pi accumulation under Pi deficiency. Importantly, the loss of *PMR4*
352 affects both *PHR1*-dependent and *LPR1*-dependent processes (Fig. 3, 4) (Bates &
353 Lynch 1996; Thibaud *et al*., 2010), which have been genetically uncoupled in PSR
354 (Wang *et al*., 2010; Balzergue *et al*., 2017). Pi accumulation and anthocyanin
355 accumulation are suppressed in *phr1 phl1* (Rubio *et al.*, 2001; Bustos *et al*., 2010; Wang
356 *et al*., 2018). The shoot Pi contents and plant biomass are also reduced in *pmr4*,
357 implying that *PMR4* positively influences *PHR1/PHL1*-mediated Pi acquisition and
358 plant growth during PSR. However, over-accumulation of anthocyanin in *pmr4* (Fig. 3k,
359 l) in contrast to *phr1 phl1* (Rubio *et al.*, 2001; Bustos *et al*., 2010; Wang *et al*., 2018),
360 suggests that *PMR4* contribution is specific to the former two outputs of *PHR1/PHL1*
361 and that its loss results in exaggeration of Pi starvation. Moreover, the loss of *PMR4*
362 also strengthens inhibition of the primary root growth under Pi deficiency, only in the
363 presence of *LPR1/LPR2* (Fig. S4). The LPR1 pathway mediates callose deposition at
364 SCN to inhibit the cell-to-cell movement of the transcription factor SHR, thereby
365 suppressing the cell division and subsequent root elongation (Müller *et al*., 2015; Mora-
366 Macías *et al*., 2017). Our results thus indicate that the callose depositions in root hairs
367 and SCN positively and negatively influence the primary root growth, respectively. The
368 two callose induction events of the opposing effects on the root growth may serve to
369 finetune the root system architecture and functioning during PSR, a hypothesis that
370 requires further studies including the identification of the SCN callose synthase. *PMR4*-
371 mediated primary root growth retention is prominent only in the presence of

372 *LPR1/LPR2*, whereas *LPR1/LPR2*-mediated growth inhibition is significant even in the
373 absence of *PMR4* under low Pi (Fig. S4). Our results imply that *PMR4* also modulates
374 *LPR1/LPR2*-dependent root growth inhibition.

375 Shoot Pi accumulation depends on root Pi uptake and subsequent Pi translocation.
376 *PHT1;1* and *PHT1;4* provide two major Pi transporters in roots, contributing greatly to
377 Pi acquisition under Pi deficiency (Shin *et al*., 2004). *PHO1* mediates Pi translocation
378 from roots to shoots through Pi loading into the root xylem (Poirier *et al.,* 1991;
379 Hamburger *et al*., 2002; Liu *et al*., 2012). Notably, the loss of *PMR4* results in a
380 decrease in the shoot Pi contents without affecting the root Pi contents (Fig. 4).
381 Likewise, the loss of *PHR1/PHL1* and *PHO1* also lowers shoot Pi contents without
382 reducing root Pi contents (Fig. 4; Liu *et al*., 2012; Wang *et al*., 2018). In *pht1;1 pht1;4*,
383 a decrease of Pi uptake in roots is associated with that of Pi translocation to the shoots
384 and shoot Pi contents (Shin *et al*., 2004). An intimate linkage between root uptake and
385 root-to-shoot translocation is also seen for K^+ (Nieves-Cordones *et al*., 2019). It is thus
386 conceivable that the lowered Pi accumulation in *pmr4* shoots is caused by a decrease in
387 the rates of the root Pi uptake and the root-to-shoot Pi translocation, possibly through
388 the compromised root hair function in the absence of *PMR4*. Indeed, ^{32}P tracer analyses
389 indicate that *PMR4* promotes both root Pi uptake and root-to-shoot Pi translocation,
390 without affecting the root Pi contents (Fig. 4). This is consistent with the view that the
391 root-to-shoot Pi translocation is driven by the Pi uptake in the roots (Shin *et al*., 2004).
392 Leaf transpiration affects root-to-shoot solute translocation (Nieves-Cordones *et al*.,
393 2019), but it should be ignorable under high humidity in the closed plate assays.

394 Root hairs increase the root surface area to promote root anchorage, nutrient
395 acquisition, and metabolite exudation, thereby facilitating the interactions with the soil

396 environments (Datta *et al*., 2011; Poole *et al*., 2018; Robe *et al*., 2021; Vissenberg *et al*.,
397 2020; Han *et al.,* 2023). As a key interface to soil-borne microbes and pests, it is
398 becoming apparent that root hairs are intimately associated with root defense activation.
399 Root hair formation and elongation are facilitated by jasmonate (JA) (Zhu *et al*., 2006),
400 which mediates the expression of key transcription factors for root hair differentiation
401 and the de-repression of RHD6 from the interference by JAZ proteins (Han *et al*, 2020).
402 In beneficial interactions with the epiphytic bacterium *Pseudomonas simiae* WCS417,
403 activation of defense-related genes is increased in hair cell lineages compared to non-
404 hair cell lineages, in a manner dependent on the root hair density (Verbon *et al*., 2023).
405 Moreover, the endogenous elicitor-active Pep peptides induce root hair formation, and
406 Pep receptor signaling from the root hairs can activate defense responses without root
407 growth inhibition (Okada *et al*., 2021), pointing to a specific capacity of root hair cells
408 in root immunity. How these properties of root hairs are influenced by *PMR4*-mediated
409 callose deposition during PSR and biotic interactions represents an interesting topic for
410 future studies.

411 Notably, PSR regulators have been implicated in the regulation of plant immunity.
412 High activation of SA-based defense and bacterial resistance occurs in *phr1 phl1*
413 (Castrillo *et al*., 2017; Motte & Beeckman, 2017). Inositol polyphosphate kinases,
414 maintaining Pi-homeostasis and PSR, also modulate crosstalk between SA-dependent
415 immunity and PSR (Kuo *et al*., 2018; Dong *et al*., 2019; Gulabani *et al*., 2022). *PMR4*-
416 dependent callose deposition in PTI provides a defense barrier, which need to be
417 overcome by bacterial pathogens through virulence-promoting effectors (Underwood *et*
418 *al*., 2007; Zhang *et al*., 2007). *pmr4* plants display an enhanced state of pathogen
419 resistance, which has been considered as a backup defense mounted when the cell wall

420 defense is subverted. In this respect, as high Pi availability often favors pathogen
421 growth and plant diseases (Paries & Gutjahr, 2023), it is conceivable that the host
422 defects in Pi acquisition and relocation to the infection sites in part contribute to the
423 lowered susceptibility to (hemi-)biotrophic pathogens in *pmr4* as well as in *phr1 phl1*
424 and *pht1;1 pht1;4* (Castrillo *et al*., 2017; Dindas *et al*., 2022). It is fascinating to
425 investigate into the mechanisms that integrate PSR and immunity signaling according to
426 the Pi and microbial infection states.
427

428 **Acknowledgement**

429 We thank the Arabidopsis Biological Research Centre for published plant materials,
430 Yaichi Kawakatsu for advice on micrografting and Michiko Tsukamoto for technical
431 assistance. This work was supported in part by the grants from Mitsubishi Foundation
432 (YS), the Japan Science and Technology Agency (JST, JPMJPR13B6 and JPMJSC1702
433 (YS) and JPMJPR16Q7 (KH)), and MEXT of Japan 18H02467 and 21H02507 (YS).
434

435 **Author contribution**

436 YS conceived the study. KO and YS designed the experiments. KO, KY, TANN, SK,
437 CT, THL, UN, KM and TM developed the methods, performed the experiments, and/or
438 analyzed the data. SM, MN and KH advised on the experiments. KO and YS wrote the
439 manuscript with contributions from the other authors.
440

441 **References**

442 **Ames BN**. **1966**. [10] Assay of inorganic phosphate, total phosphate and phosphatases.
443 *Methods in Enzymology* **8**: 115–118.

Balzergue C, Dartevelle T, Godon C, Laugier E, Meisrimler C, Teulon JM, Creff A, Bissler M, Brouchoud C, Hagège A, *et al.* **2017** Low phosphate activates STOP1-ALMT1 to rapidly inhibit root cell elongation. *Nat Commun.* doi: 10.1038/ncomms15300.

Bates TR, Lynch JP. **1996**. Stimulation of root hair elongation in *Arabidopsis thaliana* by low phosphorus availability. *Plant, Cell and Environment* **19**: 529–538.

Brouwer M, Lievens B, Van Hemelrijck W, Van Den Ackerveken G, Cammue BPA, Thomma BPHJ. **2003**. Quantification of disease progression of several microbial pathogens on *Arabidopsis thaliana* using real-time fluorescence PCR. *FEMS Microbiology Letters* **228**: 241–248.

Bustos R, Castrillo G, Linhares F, Puga MI, Rubio V, Pérez-Pérez J, Solano R, Leyva A, Paz-Ares J. **2010**. A central regulatory system largely controls transcriptional activation and repression responses to phosphate starvation in Arabidopsis. *PLoS Genetics* **6**: e1001102.

Castrillo G, Teixeira PJPL, Paredes SH, Law TF, De Lorenzo L, Feltcher ME, Finkel OM, Breakfield NW, Mieczkowski P, Jones CD, *et al.* 2017. Root microbiota drive direct integration of phosphate stress and immunity. *Nature* **543**: 513–518.

Chan C, Liao YY, Chiou TJ. 2021. The Impact of Phosphorus on Plant Immunity. *Plant and Cell Physiology* **62**: 582–589

Chien PS, Chiang CP, Leong SJ, Chiou TJ. **2018**. Sensing and Signaling of Phosphate Starvation: From Local to Long Distance. *Plant and Cell Physiology* **59**: 1714–1722.

Chowdhury J, Henderson M, Schweizer P, Burton RA, Fincher GB, Little A. **2014**.

468 Differential accumulation of callose, arabinoxylan and cellulose in
469 nonpenetrated versus penetrated papillae on leaves of barley infected with
470 *Blumeria graminis* f. sp. *hordei*. *New Phytologist* **204**: 650–660.
471 **Datta S, Kim CM, Pernas M, Pires ND, Proust H, Tam T, Vijayakumar P, Dolan**
472 **L**. **2011**. Root hairs: Development, growth and evolution at the plant-soil
473 interface. *Plant and Soil* **346**: 1–14.
474 **Dindas J, DeFalco TA, Yu G, Zhang L, David P, Bjornson M, Thibaud MC,**
475 **Custódio V, Castrillo G, Nussaume L, *et al.* 2022**. Direct inhibition of
476 phosphate transport by immune signaling in *Arabidopsis*. *Current Biology* **32**:
477 488-495.e5.
478 **Dolan L, Duckett CM, Grierson C, Linstead P, Schneider K, Lawson E, Dean C,**
479 **Poethig S, Roberts K**. **1994**. Clonal relationships and cell patterning in the
480 root epidermis of Arabidopsis. *Development* **120**: 2465–2474.
481 **Dong J, Ma G, Sui L, Wei M, Satheesh V, Zhang R, Ge S, Li J, Zhang TE, Wittwer**
482 **C, *et al.* 2019**. Inositol Pyrophosphate InsP8 Acts as an Intracellular Phosphate
483 Signal in Arabidopsis. *Molecular Plant* **12**: 1463–1473.
484 **Dong X, Hong Z, Sivaramakrishnan M, Mahfouz M, Verma DPS**. **2005**. Callose
485 synthase (CalS5) is required for exine formation during microgametogenesis
486 and for pollen viability in Arabidopsis. *Plant Journal* **42**: 315–328.
487 **Ellinger D, Voigt CA**. **2014**. Callose biosynthesis in Arabidopsis with a focus on
488 pathogen response: What we have learned within the last decade. *Annals of*
489 *Botany* **114**: 1349–1358.
490 **Enns LC, Kanaoka MM, Torii KU, Comai L, Okada K, Cleland RE**. **2005**. Two

491 callose synthases, GSL1 and GSL5, play an essential and redundant role in
492 plant and pollen development and in fertility. *Plant Molecular Biology* **58**:
493 333–349.
494 **Gulabani H, Goswami K, Walia Y, Roy A, Noor JJ, Ingole KD, Kasera M, Laha D,**
495 **Giehl RFH, Schaaf G, *et al.* 2022**. Arabidopsis inositol polyphosphate kinases
496 IPK1 and ITPK1 modulate crosstalk between SA-dependent immunity and
497 phosphate-starvation responses. *Plant Cell Reports* **41**: 347–363.
498 **Hamburger D, Rezzonico E, Petétot JMDC, Somerville C, Poirier Y**. **2002**.
499 Identification and characterization of the Arabidopsis *PHO1* gene involved in
500 phosphate loading to the xylem. *Plant Cell* **14**: 889–902.
501 **Han G, Wei X, Dong X, Wang C, Sui N, Guo J, Yuan F, Gong Z, Li X, Zhang Y, *et***
502 ***al.* 2020**. Arabidopsis ZINC FINGER PROTEIN1 Acts Downstream of GL2 to
503 Repress Root Hair Initiation and Elongation by Directly Suppressing bHLH
504 Genes. *The Plant cell* **32**: 206–225.
505 **Han X, Kui M, He K, Yang M, Du J, Jiang Y, Hu Y**. **2023**. Jasmonate-regulated root
506 growth inhibition and root hair elongation. *Journal of Experimental Botany* **74**:
507 1176–1185.
508 **Holz M, Zarebanadkouki M, Kuzyakov Y, Pausch J, Carminati A**. **2018**. Root hairs
509 increase rhizosphere extension and carbon input to soil. *Annals of Botany* **121**:
510 61–69.
511 **Isidra-Arellano MC, Delaux PM, Valdés-López O. 2021.** The Phosphate Starvation
512 Response System: Its Role in the Regulation of Plant–Microbe Interactions.
513 *Plant Cell Physiol* **62**: 392–400

514 **Jacobs AK, Lipka V, Burton RA, Panstruga R, Strizhov N, Schulze-Lefert P,**
515 **Fincher GB**. **2003**. An Arabidopsis Callose Synthase, GSL5, Is Required for
516 Wound and Papillary Callose Formation. *Plant Cell* **15**: 2503–2513.
517 **Kuo HF, Hsu YY, Lin WC, Chen KY, Munnik T, Brearley CA, Chiou TJ**. **2018**.
518 Arabidopsis inositol phosphate kinases IPK1 and ITPK1 constitute a metabolic
519 pathway in maintaining phosphate homeostasis. *Plant Journal* **95**: 613–630.
520 **Liu TY, Huang TK, Tseng CY, Lai YS, Lin SI, Lin WY, Chen JW, Chioua TJ**.
521 **2012**. PHO2-dependent degradation of PHO1 modulates phosphate
522 homeostasis in *Arabidopsis*. *Plant Cell* **24**: 2168–2183.
523 **Mateo A, Funck D, Mühlenbock P, Kular B, Mullineaux PM, Karpinski S. 2006**.
524 Controlled levels of salicylic acid are required for optimal photosynthesis and
525 redox homeostasis. *J Exp Bot* **57**: 1795–1807
526 **Mita S, Murano N, Akaike M, Nakamura K. 1997.** Mutants of *Arabidopsis thaliana*
527 with pleiotropic effects on the expression on the gene for β-amylase and on
528 the accumulation that are inducible by sugars. *Plant Journal* **97**:1087-1093.
529 **Miura K, Lee J, Miura T, Hasegawa PM. 2010**. *SIZ1*controls cell growth and plant
530 development in Arabidopsis through salicylic acid. *Plant Cell Physiol* **51**: 103–
531 113
532 **Miwa K, Wakuta S, Takada S, Ide K, Takano J, Naito S, Omori H, Matsunaga T,**
533 **Fujiwara T**. **2013**. Roles of BOR2, a boron exporter, in cross linking of
534 rhamnogalacturonan II and root elongation under boron limitation in
535 Arabidopsis. *Plant Physiology* **163**: 1699–1709.
536 **Mora-Macías J, Ojeda-Rivera JO, Gutiérrez-Alanís D, Yong-Villalobos L,**
537 **Oropeza-Aburto A, Raya-González J, Jiménez-Domínguez G, Chávez-**

538 **Calvillo G, Rellán-Álvarez R, Herrera-Estrell L**. **2017**. Malate-dependent Fe
539 accumulation is a critical checkpoint in the root developmental response to low
540 phosphate. *Proceedings of the National Academy of Sciences of the United*
541 *States of America* **114**: E3563–E3572.
542 **Morcillo RJ, Singh SK, He D, An G, Vílchez JI, Tang K, Yuan F, Sun Y, Shao C,**
543 **Zhang S, *et al.* 2020**. Rhizobacterium-derived diacetyl modulates plant
544 immunity in a phosphate-dependent manner. *The EMBO Journal* **39**: 1–15.
545 **Motte H, Beeckman T**. **2017**. PHR1 Balances between Nutrition and Immunity in
546 Plants. *Developmental Cell* **41**: 5–7.
547 **Müller J, Toev T, Heisters M, Teller J, Moore KL, Hause G, Dinesh DC,**
548 **Bürstenbinder K, Abel S**. **2015**. Iron-Dependent Callose Deposition Adjusts
549 Root Meristem Maintenance to Phosphate Availability. *Developmental Cell* **33**:
550 216–230.
551 **Nieves-Cordones M, Lara A, Ródenas R, Amo J, Rivero RM, Martínez V, Rubio F**.
552 **2019**. Modulation of K+ translocation by AKT1 and AtHAK5 in Arabidopsis
553 plants. *Plant Cell and Environment* **42**: 2357–2371.
554 **Nishikawa SI, Zinkl GM, Swanson RJ, Maruyama D, Preuss D**. **2005**. Callose (β-
555 1,3 glucan) is essential for Arabidopsis pollen wall patterning, but not tube
556 growth. *BMC Plant Biology* **5**: 1–9.
557 **Nishimura MT, Stein M, Hou BH, Vogel JP, Edwards H, Somerville SC**. **2003**.
558 Loss of a callose synthase results in salicylic acid-dependent disease resistance.
559 *Science* **301**: 969–972.
560 **Okada K, Kubota Y, Hirase T, Otani K, Goh T, Hiruma K, Saijo Y**. **2021**.
561 Uncoupling root hair formation and defence activation from growth inhibition

562 in response to damage-associated Pep peptides in Arabidopsis thaliana. *New*
563 *Phytologist* **229**: 2844–2858.
564 **O'Lexy R, Kasai K, Clark N, Fujiwara T, Sozzani R, Gallagher KL**. **2018**.
565 Exposure to heavy metal stress triggers changes in plasmodesmatal
566 permeability via deposition and breakdown of callose. *Journal of Experimental*
567 *Botany* **69**: 3715–3728.
568 **Omasits U, Ahrens CH, Müller S, Wollscheid B**. **2014**. Protter: Interactive protein
569 feature visualization and integration with experimental proteomic data.
570 *Bioinformatics* **30**: 884–886.
571 **Paries M, Gutjahr C**. **2023**. The good, the bad, and the phosphate: regulation of
572 beneficial and detrimental plant-microbe interactions by the plant phosphate
573 status. *New phytologist* **239**: 29–46.
574 **Péret B, Clément M, Nussaume L, Desnos T**. **2011**. Root developmental adaptation to
575 phosphate starvation: Better safe than sorry. *Trends in Plant Science* **16**: 442–
576 450.
577 **Péret B, Desnos T, Jost R, Kanno S, Berkowitz O, Nussaume L**. **2014**. Root
578 architecture responses: In search of phosphate. *Plant Physiol* **166**: 1713–1723.
579 **Pfaffl**. **2001**. A new mathematical model for relative quantification in real-time RT-
580 PCR. *Nucleic Acids Research* **29**:2003-2007.
581 **Poirier Y, Thoma S, Somerville C, Schiefelbein J**. **1991**. A mutant of Arabidopsis
582 deficient in xylem loading of phosphate. *Plant Physiology* **97**: 1087–1093.
583 **Poole J, Day CJ, Von Itzstein M, Paton JC, Jennings MP**. **2018**. Glycointeractions in
584 bacterial pathogenesis. *Nature Reviews Microbiology* **16**: 440–452.
585 **Pound MP, French AP, Atkinson JA, Wells DM, Bennett MJ, Pridmore T**. **2013**.

586 RootNav: Navigating images of complex root architectures. *Plant Physiology*
587 **162**: 1802–1814.
588 **Robe K, Conejero G, Gao F, Lefebvre-Legendre L, Sylvestre-Gonon E, Rofidal V,**
589 **Hem S, Rouhier N, Barberon M, Hecker A, *et al.* 2021**. Coumarin
590 accumulation and trafficking in Arabidopsis thaliana: a complex and dynamic
591 process. *New Phytologist* **229**: 2062–2079.
592 **Robertson-Albertyn S, Terrazas RA, Balbirnie K, Blank M, Janiak A, Szarejko I,**
593 **Chmielewska B, Karcz J, Morris J, Hedley PE, *et al.* 2017**. Root hair
594 mutations displace the barley rhizosphere microbiota. *Frontiers in Plant*
595 *Science* **8**: 1–15.
596 **Rubio V, Linhares F, Solano R, Martín AC, Iglesias J, Leyva A, Paz-Ares J**. **2001**.
597 A conserved MYB transcription factor involved in phosphate starvation
598 signaling both in vascular plants and in unicellular algae. *Genes and*
599 *Development* **15**: 2122–2133.
600 **Sager R, Lee JY**. **2014**. Plasmodesmata in integrated cell signalling: Insights from
601 development and environmental signals and stresses. *Journal of Experimental*
602 *Botany* **65**: 6337–6358.
603 **Schenk ST, Schikora A**. **2015**. http://www.bio-protocol.org/e1429 Vol 5, Iss 6, Mar
604 20, 2015. **5**: 3–6.
605 **Schiefelbein J, Kwak SH, Wieckowski Y, Barron C, Bruex A**. **2009**. The gene
606 regulatory network for root epidermal cell-type pattern formation in
607 Arabidopsis. *Journal of Experimental Botany* **60**: 1515–1521.

608 **Shin H, Shin HS, Dewbre GR, Harrison MJ**. **2004**. Phosphate transport in
609 *Arabidopsis*: Pht1;1 and Pht1;4 play a major role in phosphate acquisition from
610 both low- and high-phosphate environments. *Plant Journal* **39**: 629–642.
611 **Stefanovic A, Ribot C, Rouached H, Wang Y, Chong J, Belbahri L, Delessert S,**
612 **Poirier Y**. **2007**. Members of the PHO1 gene family show limited functional
613 redundancy in phosphate transfer to the shoot, and are regulated by phosphate
614 deficiency via distinct pathways. *Plant Journal* **50**: 982–994.
615 **Sun L, Song L, Zhang Y, Zheng Z, Liu D**. **2016**. Arabidopsis PHL2 and PHR1 act
616 redundantly as the key components of the central regulatory system controlling
617 transcriptional responses to phosphate starvation. *Plant Physiology* **170**: 499–
618 514.
619 **Svistoonoff S, Creff A, Reymond M, Sigoillot-Claude C, Ricaud L, Blanchet A,**
620 **Nussaume L, Desnos T**. **2007**. Root tip contact with low-phosphate media
621 reprograms plant root architecture. *Nat Genet* **39**: 792–796
622 **Tanaka N, Kato M, Tomioka R, Kurata R, Fukao Y, Aoyama T, Maeshima M**.
623 **2014**. Characteristics of a root hair-less line of *Arabidopsis thaliana* under
624 physiological stresses. *Journal of Experimental Botany* **65**: 1497–1512.
625 **Thibaud MC, Arrighi JF, Bayle V, Chiarenza S, Creff A, Bustos R, Paz-Ares J,**
626 **Poirier Y, Nussaume L**. **2010**. Dissection of local and systemic transcriptional
627 responses to phosphate starvation in Arabidopsis. *Plant Journal* **64**: 775–789.
628 **Underwood W, Zhang S, He SY**. **2007**. The *Pseudomonas syringae* type III effector
629 tyrosine phosphatase HopAO1 suppresses innate immunity in *Arabidopsis*
630 *thaliana*. *Plant Journal* **52**: 658–672.

631 **Verbon EH, Liberman LM, Zhou J, Yin J, Pieterse CMJ, Benfey N, Stringlis IA,**
632 **Jonge R De**. **2023**. Cell type-specific transcriptomics reveals that root hairs
633 and endodermal barriers play important roles in beneficial plant-
634 rhizobacterium-interactions. *MOLECULAR PLANT* doi:
635 https://doi.org/10.1016/j.molp.2023.06.001.
636 **Vissenberg K, Claeijs N, Balcerowicz D, Schoenaers S**. **2020**. Hormonal regulation of
637 root hair growth and responses to the environment in Arabidopsis. *Journal of*
638 *Experimental Botany* **71**: 2412–2427.
639 **Vogel J, Somerville S. 2000**. Isolation and characterization of powdery mildew-
640 resistant *Arabidopsis* mutants. *PNAS* **97**: 1897–1902.
641 **Wang X, Du G, Wang X, Meng Y, Li Y, Wu P, Yi K**. **2010**. The function of LPR1 is
642 controlled by an element in the promoter and is independent of SUMO E3
643 ligase SIZ1 in response to Low Pi stress in *Arabidopsis thaliana*. *Plant and*
644 *Cell Physiology* **51**: 380–394.
645 **Wang Z, Zheng Z, Song L, Liu D**. **2018**. Functional characterization of Arabidopsis
646 PHL4 in plant response to phosphate starvation. *Frontiers in Plant Science* **9**:
647 1–19.
648 **Wang Y, Li X, Fan B, Zhu C, Chen Z. 2021**. Regulation and function of defense-
649 related callose deposition in plants. *Int J Mol Sci* **22**: 1–15.
650 **Weßling R, Panstruga R**. **2012**. Rapid quantification of plant-powdery mildew
651 interactions by qPCR and conidiospore counts. *Plant Methods* **8**.
652 **Wildermuth MC, Dewdney J, Wu G, Ausubel FM**. **2002**. Erratum: corrigendum:
653 Isochorismate synthase is required to synthesize salicylic acid for plant
654 defense. *Nature* **417**: 571–571.

655 **Wu SW, Kumar R, Iswanto ABB, Kim JY**. **2018**. Callose balancing at
656 plasmodesmata. *Journal of Experimental Botany* **69**: 5325–5339.
657 **Zhang J, Shao F, Li Y, Cui H, Chen L, Li H, Zou Y, Long C, Lan L, Chai J, *et al.***
658 **2007**. A *Pseudomonas syringae* Effector Inactivates MAPKs to Suppress
659 PAMP-Induced Immunity in Plants. *Cell Host Microbe* **1**: 175–185
660 **Zhang X, Chen S, Mou Z. 2010**. Nuclear localization of NPR1 is required for
661 regulation of salicylate tolerance, isochorismate synthase 1 expression and
662 salicylate accumulation in Arabidopsis. *J Plant Physiol* **167**: 144–148
663 **Zhu C, Gan L, Shen Z, Xia K**. **2006**. Interactions between jasmonates and ethylene in
664 the regulation of root hair development in Arabidopsis. *Journal of*
665 *Experimental Botany* **57**: 1299–1308.
666

667 **Figure Legends**

668 **Fig.1 Callose deposition is induced in root hairs under phosphate deficiency,**
669 **independently of *PHR1, PHL1, LPR1* and *LPR2*.**

670 Aniline blue staining of the primary roots 3 d after transfer of 5-d-old *Arabidopsis*
671 *thaliana* seedlings to low Pi (P 50 μM), low N (N 0 μM), low Fe (Fe 0 μM), low Fe low
672 Pi (Fe 0 μM, P 0 μM) or normal Pi (P 625 μM) liquid media. (a, c, left) Bright field
673 (BF) images. (a, c, right) Aniline blue staining images. White arrows indicate root hair
674 tips. (b) Aniline blue staining of root hairs under low Pi and normal Pi conditions. (c)
675 The wild-type (WT) used for *rhd6* was Ws-2. (a, c, lower panel) Magnified images of
676 (a, c, upper panel). Bar, 500 μm (a, c, upper panel), 50 μm (a, c lower panel) and 25 μm
677 (b).
678

679 **Fig. 2 Callose synthase *PMR4* is required for callose induction under phosphate**
680 **deficiency.**
681 (a) Aniline blue staining of the primary roots 3 d after transfer of 5-d-old *Arabidopsis*
682 *thaliana* plants to low Pi (0 μM) liquid media. (a, left) Bright filed (BF) images. (a,
683 right) Aniline blue staining images. Two *caps* mutants are defective in inducing *callose*
684 *under phosphate starvation.* (a, lower panel) Magnified images of (a, upper panel).
685 White arrows indicate root hair tips. Bar, 500 μm (A, upper panel) or 50 μm (a, lower
686 panel). (b) Positions of mutated sites in the *PMR4* locus of *caps* mutants, illustrated
687 with Protter (Omasits *et al*., 2014). An orange region corresponds to the catalytic
688 domain of PMR4. Asterisks indicate stop codons. (c) Leaves 10 d after inoculation with
689 *Golovinomyces orontii*. Bar, 2 cm. (d) Ratios of *G. orontii* genomic DNA to *A. thaliana*
690 genomic DNA were determined by qPCR with the primers for Plasma membrane
691 ATPase 1 (Go_V1_Conting3757) and RNA-binding family protein (AT3G21215),
692 respectively. Data show means ± SD (n=3). Asterisks (** $P < 0.01$) indicate statistically
693 significant differences relative to WT according to Student's *t*-test.
694
695 **Fig. 3 *PMR4* modulates phosphate starvation responses in the roots and shoots.**
696 (a) Aniline blue staining of the primary roots 3 d after transfer of 5-d-old *Arabidopsis*
697 *thaliana* seedlings to low Pi (50 μM) liquid media. (left) Bright filed (BF) images.
698 (right) Aniline blue staining images. (lower panel) Magnified images of (upper panel).
699 White arrows indicate root hair tips. Bar, 100 μm (upper panel) or 50 μm (lower panel).
700 (b) Six-d-old seedlings were exposed to low Pi (50 μM) or normal Pi (625 μM) media
701 for 6 d. Bars, 10 mm. (c) The primary roots 9 d after transfer of 6-d-old seedling to low
702 Pi (50 μM) and normal Pi (625 μM) media. Bar, 1 mm. (d) Root hair density and root

703 hair length in (c). (e) Primary root length in (b). (f) Ratio of the primary root length
704 under normal Pi relative to low Pi of (e). (g) Convex hull area of the roots in (b). (h)
705 Ratio of convex hull area under normal Pi relative to low Pi of (g). (i) Six-d-old
706 seedlings were exposed to low Pi (50 μM) or normal Pi (625 μM) for 16 d. Bar, 10 mm.
707 (j) SFW in (i). (k) Six-d-old seedlings were exposed to low Pi (10 μM) media for 10 d.
708 Bar, 10 mm. (l) Anthocyanin contents in (k). (d-h, j, l) Data show means ± SD (n =
709 7~30). Statistical significance was assessed by one-way ANOVA and Tukey honestly
710 significant different (HSD) test for each medium dataset. Different letters indicate
711 significant differences ($P < 0.05$). NS, not significant.
712
713 **Fig. 4 *PMR4* contributes to shoot growth and Pi accumulation under phosphate**
714 **deficiency**
715 (a-d) Pi contents per root or shoot fresh weight (FW) of 6-d-old *Arabidopsis thaliana*
716 seedlings exposed to low Pi (150 μM) or normal Pi (625 μM) for 9 d. (e) Illustration of
717 Pi accumulation in the indicated genotypes, referred to (a-d). (f) ^{32}P uptake rate
718 determined in the whole seedlings exposed to the indicated media (low Pi and normal
719 Pi, 50 and 625 μM Pi, respectively) supplemented with ^{32}P-labelled Pi for 30 min. (g)
720 Ratio of ^{32}P in the shoots relative to the whole plants after pulse-chase labeling.
721 Seedlings grown on low and normal Pi media (50 and 625 μM, respectively) were
722 exposed to ^{32}P-labeled Pi for 10 min, and then transferred to non-labelled Pi media for
723 120 min (pulse chase). The ^{32}P ratio of the shoots to the whole seedlings was calculated
724 for the translocation rate of Pi. (a-d, f-g) Data show means ± SD (n = 3~4). (a-b, f-g)
725 Statistical significance was assessed by one-way ANOVA and Tukey HSD test for each
726 medium dataset. Different letters indicate significant differences ($P < 0.05$). (c, d)

727 Asterisks (** $P < 0.01$, * $P < 0.05$) indicate statistically significant differences relative
728 to WT according to Student's *t*-test. NS, not significant.
729
730 **Fig. 5 Root *PMR4* contributes to shoot growth under phosphate deficiency.**
731 (a) Reciprocal micrografting of *Arabidopsis thaliana* WT and *pmr4* mutants. Images
732 were obtained at 14 d after transfer to low Pi (150 μM) media. Bar, 10 mm. (b) Shoot
733 fresh weight (SFW) of (a). (c) The primary root length of (a). (d) Aniline blue staining
734 of grafted-seedlings at 9 d after transfer to low Pi (50 μM). (d, left) Bright filed (BF)
735 images. (d, right) Aniline blue staining images. (d, lower panel) Magnified images of (d,
736 upper panel). White arrows indicate root hair tips. Bar, 100 μm (c, upper panel) or 20
737 μm (c, lower panel). (b, c) Data show means ± SD (n=19-26). Statistical significance
738 was assessed by one-way ANOVA and Tukey HSD test for each medium dataset.
739 Different letters indicate significant differences ($P < 0.05$).
740
741 **Fig. 6 A model for PMR4-mediated adaptation to Pi deficiency**
742 *PMR4* induces callose deposition in root hairs under phosphate deficiency, and thus
743 contributes to shoot Pi accumulation and growth through enhancing Pi uptake and root-
744 to-shoot transfer. This contribution alleviates phosphate starvation traits, such as root
745 system area reduction and anthocyanin accumulation.
746
747 **Supporting information**
748 **Fig. S1 Callose deposition in *gsl* mutants under phosphate deficiency**

749 **Fig. S2 flg22-induced callose deposition is impaired in the *caps* and *pmr4* alleles.**

750 **Fig. S3 Primary root growth inhibition in response to B deficiency is not affected in**

751 ***pmr4*.**

752 **Fig. S4 *PMR4* restricts *LPR1/LPR2*-mediated inhibition of the primary root growth**

753 **in response to low Pi.**

754 **Fig. S5 Plant growth is lowered in *pmr4* on soil.**

755 **Table S1 *Arabidopsis thaliana* mutants used in this study**

756 **Table S2 DNA Primers used in qPCR analyses**

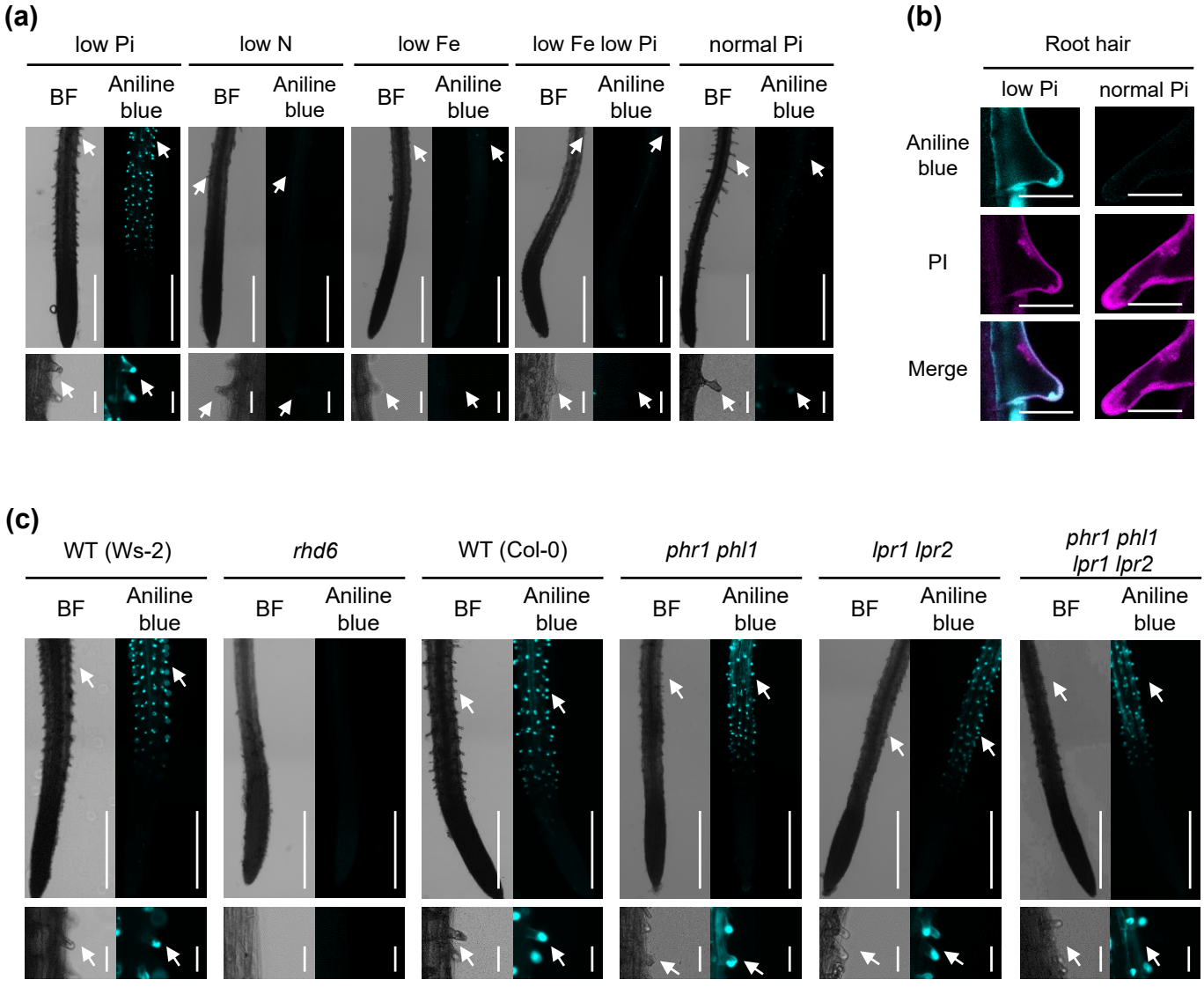

Fig.1 Callose deposition is induced in root hairs under phosphate deficiency, independently of *PHR1, PHL1, LPR1* and *LPR2*.

Aniline blue staining of the primary roots 3 d after transfer of 5-d-old *Arabidopsis thaliana* seedlings to low Pi (P 50 µM), low N (N 0 µM), low Fe (Fe 0 µM), low Fe low Pi (Fe 0 µM, P 0 µM) or normal Pi (P 625 µM) liquid media. (a, c, left) Bright field (BF) images. (a, c, right) Aniline blue staining images. White arrows indicate root hair tips. (b) Aniline blue staining of root hairs under low Pi and normal Pi conditions. (c) The wild-type (WT) used for *rhd6* was Ws-2. (a, c, lower panel) Magnified images of (a, c, upper panel). Bar, 500 µm (a, c, upper panel), 50 µm (a, c lower panel) and 25 µm (b).

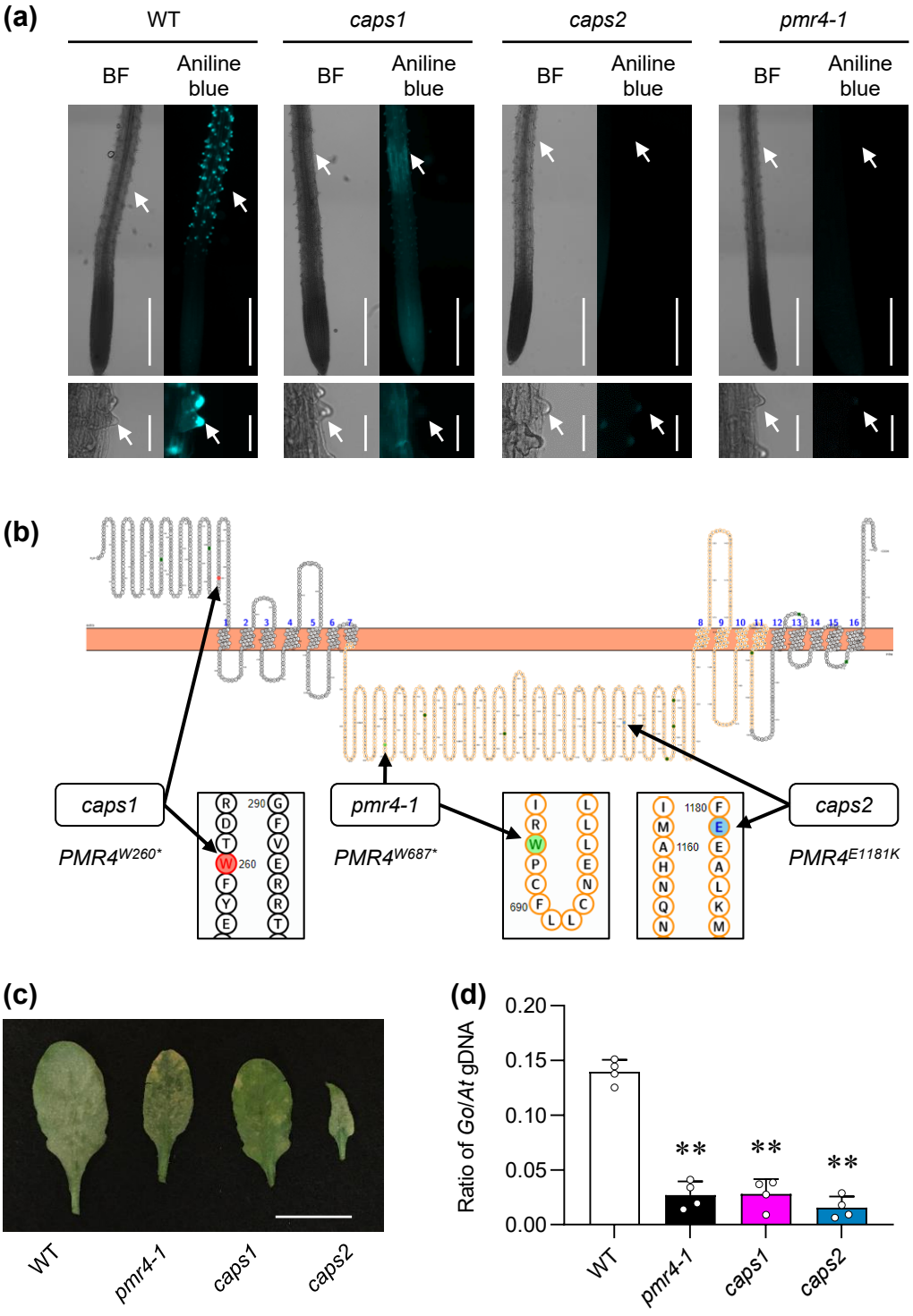

Fig. 2. Callose synthase *PMR4* is required for callose induction under phosphate deficiency.

(a) Aniline blue staining of the primary roots 3 d after transfer of 5-d-old *Arabidopsis thaliana* plants to low Pi (0 µM) liquid media. (a, left) Bright filed (BF) images. (a, right) Aniline blue staining images. Two *caps* mutants are defective in inducing *callose under phosphate starvation.* (a, lower panel) Magnified images of (a, upper panel). White arrows indicate root hair tips. Bar, 500 µm (A, upper panel) or 50 µm (a, lower panel). (b) Positions of mutated sites in the *PMR4* locus of *caps* mutants, illustrated with Protter (Omasits *et al*., 2014). An orange region corresponds to the catalytic domain of PMR4. Asterisks indicate stop codons. (c) Leaves 10 d after inoculation with *Golovinomyces orontii*. Bar, 2 cm. (d) Ratios of *G. orontii* genomic DNA to *A. thaliana* genomic DNA were determined by qPCR with the primers for Plasma membrane ATPase 1 (Go_V1_Conting3757) and RNA-binding family protein (AT3G21215), respectively. Data show means ± SD (n=3). Asterisks (** $P < 0.01$) indicate statistically significant differences relative to WT according to Student's *t*-test.

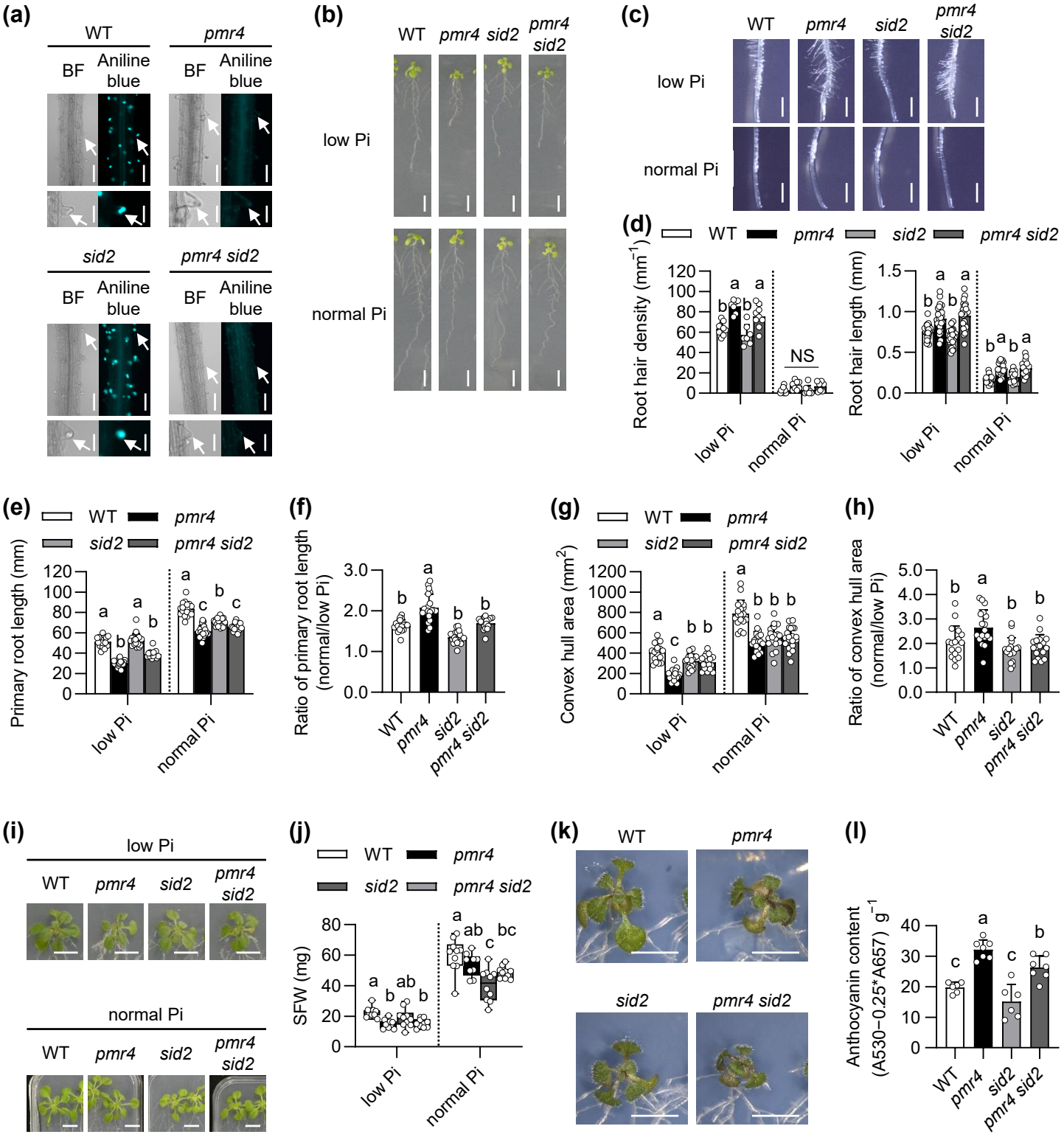

Fig. 3 *PMR4* modulates phosphate starvation response in root and shoot.

(a) Aniline blue staining of the primary roots 3 d after transfer of 5-d-old *Arabidopsis thaliana* seedlings to low Pi (50 μM) liquid media. (left) Bright filed (BF) images. (right) Aniline blue staining images. (lower panel) Magnified images of (upper panel). White arrows indicate root hair tips. Bar, 100 μm (upper panel) or 50 μm (lower panel). (b) Six-d-old seedlings were exposed to low Pi (50 μM) or normal Pi (625 μM) media for 6 d. Bars, 10 mm. (c) The primary roots 9 d after transfer of 6-d-old seedling to low Pi (50 μM) and normal Pi (625 μM) media. Bar, 1 mm. (d) Root hair density and root hair length in (c). (e) Primary root length in (b). (f) Ratio of the primary root length under normal Pi relative to low Pi of (e). (g) Convex hull area of the roots in (b). (h) Ratio of convex hull area under normal Pi relative to low Pi of (g). (i) Six-d-old seedlings were exposed to low Pi (50 μM) or normal Pi (625 μM) for 16 d. Bar, 10 mm. (j) SFW in (i). (k) Six-d-old seedlings were exposed to low Pi (10 μM) media for 10 d. Bar, 10 mm. (l) Anthocyanin contents in (k). (d-h, j, l) Data show means ± SD (n = 7~30). Statistical significance was assessed by one-way ANOVA and Tukey honestly significant different (HSD) test for each medium dataset. Different letters indicate significant differences ($P < 0.05$). NS, not significant.

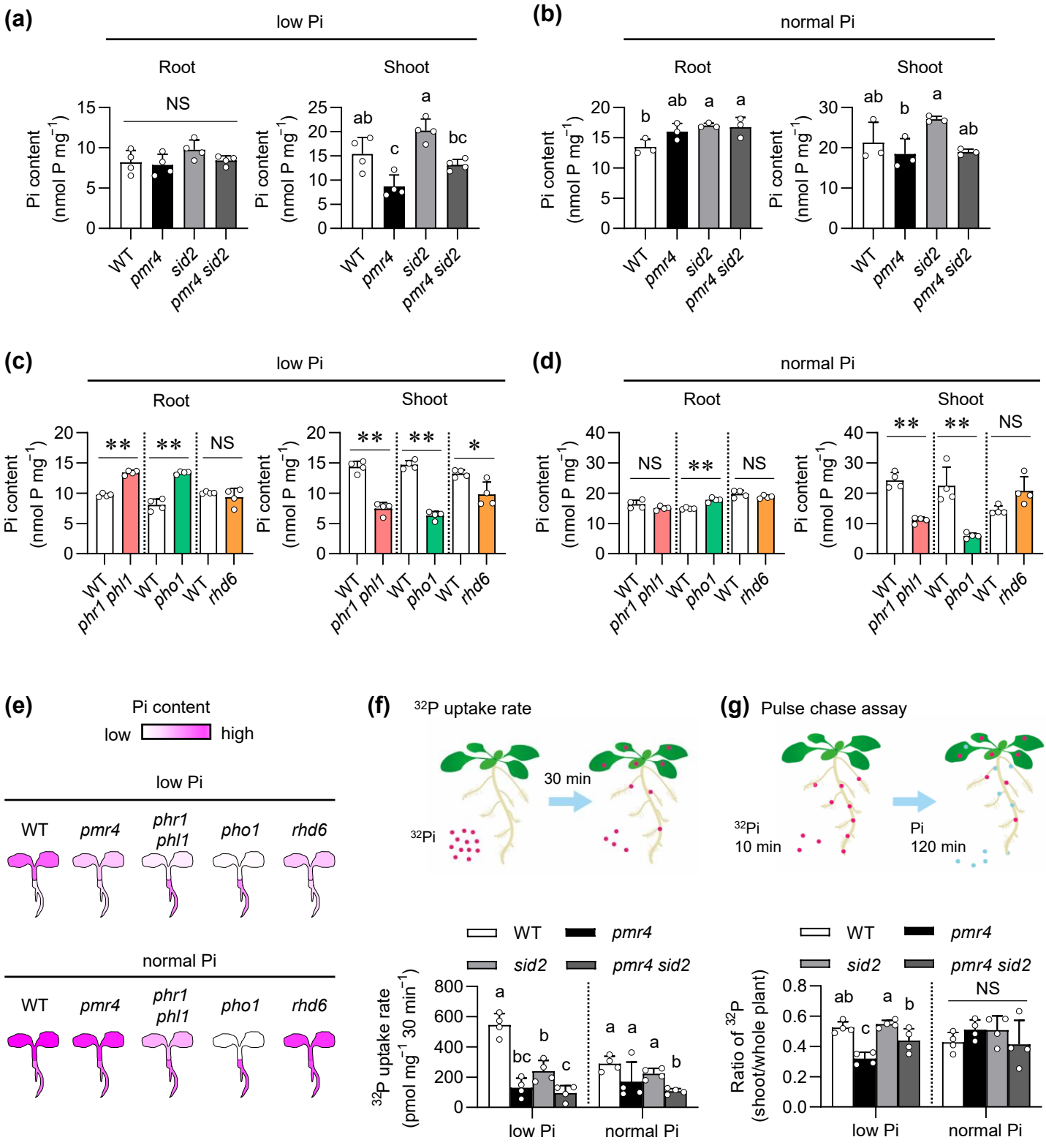

Fig. 4 *PMR4* contributes to shoot growth and Pi accumulation under phosphate deficiency

(a-d) Pi contents per root or shoot fresh weight (FW) of 6-d-old *Arabidopsis thaliana* seedlings exposed to low Pi (150 μM) or normal Pi (625 μM) for 9 d. (e) Illustration of Pi accumulation in the indicated genotypes, referred to (a-d). (f) ^{32}P uptake rate determined in the whole seedlings exposed to the indicated media (low Pi and normal Pi, 50 and 625 μM Pi, respectively) supplemented with ^{32}P-labelled Pi for 30 min. (g) Ratio of ^{32}P in the shoots relative to the whole plants after pulse-chase labeling. Seedlings grown on low and normal Pi media (50 and 625 μM, respectively) were exposed to ^{32}P-labeled Pi for 10 min, and then transferred to non-labelled Pi media for 120 min (pulse chase). The ^{32}P ratio of the shoots to the whole seedlings was calculated for the translocation rate of Pi. (a-d, f-g) Data show means ± SD (n = 3~4). (a-b, f-g) Statistical significance was assessed by one-way ANOVA and Tukey HSD test for each medium dataset. Different letters indicate significant differences ($P < 0.05$). (c, d) Asterisks (** $P < 0.01$, * $P < 0.05$) indicate statistically significant differences relative to WT according to Student's *t*-test. NS, not significant.

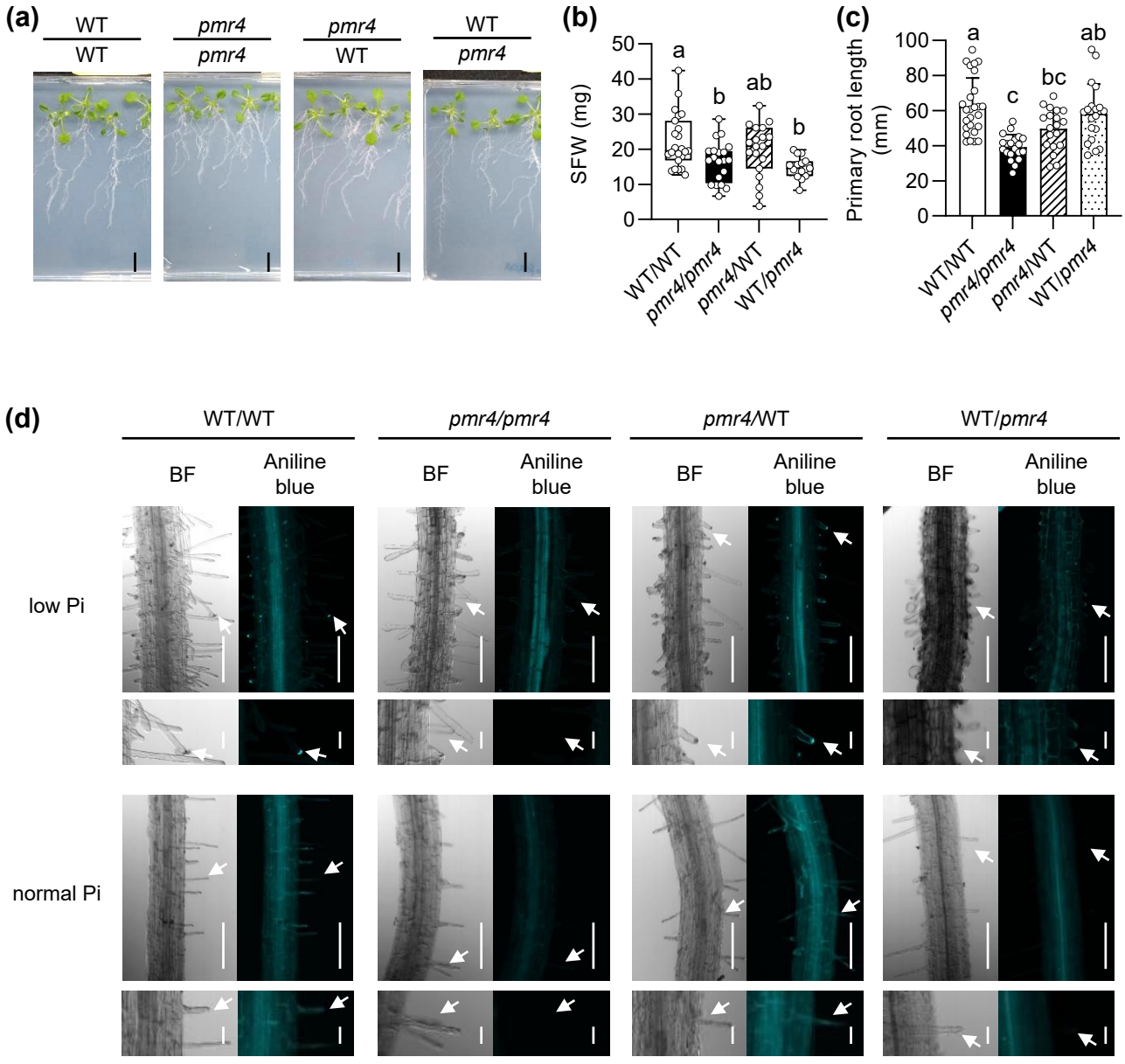

Fig. 5 Root *PMR4* contributes to shoot growth under phosphate deficiency.

(a) Reciprocal micrografting of *Arabidopsis thaliana* WT and *pmr4* mutants. Images were obtained at 14 d after transfer to low Pi (150 µM) media. Bar, 10 mm. (b) Shoot fresh weight (SFW) of (a). (c) The primary root length of (a). (d) Aniline blue staining of grafted-seedlings at 9 d after transfer to low Pi (50 µM). (d, left) Bright filed (BF) images. (d, right) Aniline blue staining images. (d, lower panel) Magnified images of (d, upper panel). White arrows indicate root hair tips. Bar, 100 µm (c, upper panel) or 20 µm (c, lower panel). (b, c) Data show means ± SD (n=19-26). Statistical significance was assessed by one-way ANOVA and Tukey HSD test for each medium dataset. Different letters indicate significant differences ($P < 0.05$).

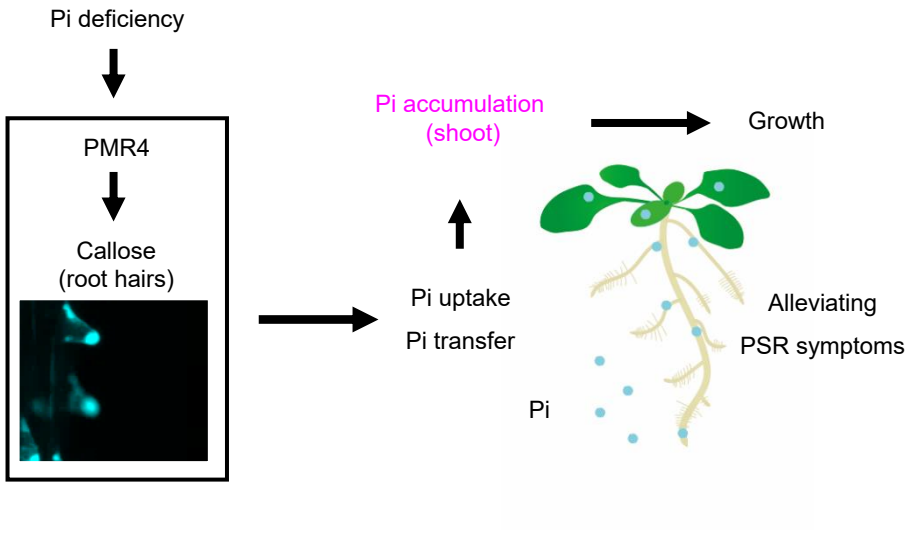

Fig. 6 Model of PMR4-mediated adaptation to Pi deficiency

PMR4 induces callose deposition in root hairs under phosphate deficiency, and thus contributes to shoot Pi accumulation and growth through enhancing Pi uptake and root-to-shoot transfer. This contribution alleviates phosphate starvation traits, such as root system area reduction and anthocyanin accumulation.